

Crystal chemistry and infrared spectroscopy in the OH-stretching region of synthetic staurolites

MONIKA KOCH-MÜLLER¹, KLAUS LANGER¹, HARALD BEHRENS², GÖTZ SCHUCK^{1,3}

¹ Institut für Angewandte Geowissenschaften I, Fachgebiet Allgemeine und Angewandte Mineralogie, Technische Universität Berlin, Ernst-Reuter-Platz 1, D-10587 Berlin
e-mail: koch1637@mailszrz.zrz.tu-berlin.de

² Institut für Mineralogie, Universität Hannover, Welfengarten 1, D-30167 Hannover

³ Present address: Hahn-Meitner-Institut, NI, Glienicker Str. 100, D-14109 Berlin

Abstract: Fe-staurolite synthesized in the pressure range 5 to 25 kbar at 680 °C was analysed by microprobe and by a titration method (for water-contents) which uses the "Karl-Fischer" reaction and also characterized by FT-infrared powder spectroscopy in the OH-stretching region (3000–4000 cm⁻¹). The study shows that the stoichiometry of the synthetic Fe-staurolites depends on the pressure of equilibration, with Fe pfu decreasing with increasing pressure, according to the heterovalent substitution of Fe²⁺ by Al³⁺ in the T2 site. This charge-increasing substitution is combined with charge-reducing substitutions in the "kyanite"-layer and by vacancies in the proton site H1. The incorporation of Al in T2 is supported by peculiarities of the IR-spectra in the range of the OH-valence vibrations.

Mg- and Zn-staurolite were synthesized at 25 kbar and 700 °C and investigated by infrared spectroscopy. The comparison of the infrared spectra of synthetic Fe-, Mg- and Zn-staurolites shows that there is a significant amount of Fe²⁺, Mg and Zn in the respective M2 sites.

Key-words: synthetic staurolites, staurolite stoichiometry, Karl-Fischer titration, infrared spectroscopy, OH-stretching region.

Introduction

In the last decade, more than twenty papers dealing with the complex crystal chemistry of natural and synthetic staurolites have been published, helping to clarify the real formula of staurolite and the main substitution mechanisms. Lonker (1983) and Holdaway *et al.* (1986a) showed that natural staurolites have variable H-contents. Holdaway *et al.* (1991 and 1995) formulated guidelines to assign site occupancies. Alexander (1989) and Dyar *et al.* (1991) investigated Fe-rich staurolites by Mössbauer spectroscopy. Dutrow (1991) experimentally determined intracrystalline distribution of Li and Al and showed that the Li incorporation in the structure is controlled by the vacancy concentration in the octahedral sites. Ståhl *et al.* (1988) and Hawthorne *et al.* (1993a,b,c) investigated the crystal structure of natural staurolites and derived the

site occupancies. Fockenberg (1995) investigated the crystal chemistry of synthetic Mg-staurolite as a function of water pressure. Staurolite syntheses were also performed by Schreyer & Seifert (1969), Griffen (1981), Phillips & Griffen (1986) and Lattard & Bubenik (1995).

On the basis of the structural investigation of natural staurolites by Hawthorne *et al.* (1993a, b,c), it is clear from the complex crystal chemistry that the ideal formula of staurolite, often referred to, Fe₄Al₁₈Si₈O₄₆(OH)₂, should be replaced by the more realistic formula M₃₋₄^[T2]Fe_{2+0-0.5}^[M4]Al₂□₂^[M3]Al₁₆^[M1,M2]Si₈^[T1]O₄₈H₂₋₄ with the crystallographic sites in square brackets (M1–M4: octahedrally coordinated, T1–T2 tetrahedrally coordinated; for details of site nomenclature see Hawthorne *et al.*, 1993a) and with M = Fe²⁺, Mg, Zn, Al and Li. Much of the Fe²⁺ and 60% of the Mg is assigned to the T2 site, while the remaining

Mg is localized in M1, M2 and M3 sites. The occupation of T2 is complicated by variable vacancy and Al-contents. A small amount of Fe²⁺ is also expected in the largely vacant M4 sites. Concerning the M1 and M2 sites, Hawthorne *et al.* (1993a) concluded that transition metals (Fe²⁺, Fe³⁺, Ti⁴⁺, Cr³⁺) are preferentially ordered in the M2 site. In a Mg-rich and concomitantly Li-rich natural staurolite investigated by Hawthorne *et al.* (1993a,b,c), the M4 site is occupied by Mg only and there are less vacancies than in the Fe-rich staurolites.

Because of the complex nature of staurolite, a closer look at synthetic phases with a restricted number of components should provide an improved understanding of the intracrystalline distribution. In this paper, we present results on the stoichiometry of Fe-staurolites synthesized at different pressures. Infrared spectroscopy in the OH-valence vibrational region of synthetic Fe-, Mg- and Zn-staurolites is used to obtain further information on the incorporation of protons in the structure and the substitution mechanisms in the proton coordinating sites T2 and M2.

Experimental procedure

Syntheses

Fe-staurolite

Preliminary synthesis runs, aimed at determining the compositions and conditions yielding single-phase Fe-staurolite, were performed at 25 and 10 kbar for 48–76 hours at 670–750 °C in a piston-cylinder apparatus (Cemic *et al.*, 1990) and at 5 kbar and 680 °C in a cold-seal vessel apparatus with water as pressure medium (run duration of 72–114 hours). All runs were buffered at the oxygen fugacity defined by the WI buffer using the double-capsule technique with an inner AgPd capsule and an outer iron capsule (in the case of the piston-cylinder technique) or an outer gold capsule (in case of the cold-seal apparatus). The buffer material consisted of wüstite synthesized in evacuated quartz-glass ampoules from a mixture of Fe metal and Fe₂O₃ powder p.a. (Merck) and metallic iron. The presence of the buffer phases was checked after the run by X-ray powder diffraction. The staurolites were synthesized under the following conditions:

- (i) 10 and 25 kbar from mixtures of Fe powder p.a. (Merck), Fe₂O₃ powder p.a. (Merck), non-crystalline SiO₂ (Aerosil 200, Degussa,

heated at 1000 °C for 48 h) and γ-Al₂O₃ (reacted from 99.95% Al foil from Merck) at different bulk compositions in combination with aqueous FeCl₂ solutions or pure water in excess.

- (ii) 10 and 25 kbar from a mixture of natural andalusite, synthetic hercynite and wüstite in a molar ratio corresponding to the composition Fe₄Al₁₈Si_{7.5}O₄₆ with aqueous FeCl₂ solution or pure water in excess.
- (iii) 10 kbar with some of the synthesis products being crushed after a first run duration of 48 h and then continued under the same conditions plus aqueous FeCl₂ solution.
- (iv) Syntheses at 5 kbar and 680 °C failed to produce Fe-staurolite from mixtures (i) and (ii); so we equilibrated the previously formed Fe-staurolite of the 10 kbar runs at 5 kbar and 680 °C with 2 molar aqueous FeCl₂ solution.

Microprobe analyses of the preliminary run products of Table 1 showed, that at a certain pressure the composition of the staurolites obtained does not depend on the bulk starting composition but additional phases (stable or metastable) may occur. However, the starting composition to achieve 100% Fe-staurolite differs with pressure. On the basis of these results, synthesis runs were optimized to yield 100% staurolite, and performed as follows:

- (i) 25 kbar and 680 °C using an oxide mixture of the composition Fe_{3.7}Al_{18.36}Si_{7.65}O_{46.5} with H₂O in excess for 48 hours.
- (ii) 10 kbar and 680 °C using an oxide mixture of the composition Fe₄Al₁₈Si_{7.5}O₄₆ with H₂O in excess for 48 hours.
- (iii) 5 kbar and 680 °C using previously formed Fe-staurolites of the 10 kbar runs equilibrated with 2 molar aqueous FeCl₂ solution for 96 hours.

These run conditions were used for all the products shown in Table 2.

Mg- and Zn-staurolites

These phases were synthesized in gold capsules from oxide mixtures at 25 kbar and 700 °C in a piston-cylinder device using MgO p.a. (Merck), ZnO p.a. (Merck), non-crystalline SiO₂ (Aerosil 200, Degussa, heated at 1000 °C for 48 h) and γ-Al₂O₃ (reacted from 99.95% Al foil from Merck). Best results were obtained on the molar basis Mg_{3.8}Al_{18.3}Si_{7.6}O_{46.45} and Zn₄Al₁₈Si_{7.5}O₄₆ for the

Table 1. Stoichiometry of synthetic Fe-staurolite, equilibrated using different bulk compositions (1 σ : standard deviation).

starting material ^c	Oxide ^a 4:9:7.5	Oxide ^a 4:9:7.5	Oxide ^a 4:9:7.5	Oxide ^a 4:9:7.5	Oxide ^a 3.7:9.18:7.5	Oxide ^a 3.7:9.18:7.5	and. + hc + wü ^b	oxide ^a 4:9:7.5	st + FeCl ₂	and + hc + wü ^b +FeCl ₂	st + chd	st + FeCl ₂
temperature [°C]	670	700	750	750	670	680	720	680	680	680	680	680
pressure [kbar]	25	25	25	25	25	25	25	10	10	10	5	5
Run duration [hours]	72	72	48	48	76	48	20	48	48	22	96	114
phases ^c	st(95) + chd	st(90) + grt	st(85)+grt ± ky?	st(95)+crn	st (95)+ cld	st	st(85)+grt ±ky?	st	st	st(90)+grt+qtz	fe-st(90) + qtz	fe-st
number of analyses	8	11	8	8	20	13	20	17	10	10	24	12
SiO ₂ wt %	27.39(96)	26.65(94)	26.53(111)	26.91(11)	26.88(85)	25.87(124)	26.82(52)	25.89(79)	26.01(66)	25.99(55)	25.04(48)	25.80(50)
Al ₂ O ₃ wt %	55.13(137)	55.53(149)	55.90(125)	54.99(23)	55.35(142)	55.97(99)	54.57(84)	54.69(121)	55.06(94)	54.89(67)	55.47(62)	54.87(101)
FeO wt % ^d	15.20 (29)	14.96(41)	14.95(22)	15.62(20)	15.40(59)	15.33(19)	15.24(14)	15.94(41)	16.35(24)	15.88(20)	16.56(40)	16.76(22)
H ₂ O wt % ^e	1.57	1.57	1.57	1.57	1.57	1.57	1.57	1.65	1.65	1.65	1.88	1.88
Σ	99.31(168)	98.71(129)	98.96(128)	99.09(13)	99.20(150)	98.78(119)	98.20(97)	98.17(88)	99.07(77)	98.19(90)	98.95(62)	99.30(97)
Si	7.72(20)	7.56(25)	7.51(26)	7.63(2)	7.60(23)	7.40(29)	7.66(12)	7.43(24)	7.41(17)	7.44(15)	7.14(12)	7.33(15)
Al	18.31(27)	18.57(37)	18.64(32)	18.37(4)	18.45(30)	18.75(36)	18.37(16)	18.49(31)	18.48(25)	18.53(23)	18.65(19)	18.38(22)
Fe	3.58(11)	3.55(12)	3.54(9)	3.70(5)	3.64(15)	3.65(7)	3.64(6)	3.82(11)	3.89(8)	3.75(11)	3.95(10)	3.98(5)
H	3.01	2.98	2.97	2.97	2.97	2.97	3.04	3.16	3.14	3.16	3.58	3.57
Σ	32.63(10)	32.65(9)	32.66(13)	32.67(2)	32.66	32.79(128)	32.66(7)	32.91(10)	32.92(6)	32.87(11)	33.32(5)	33.26(5)
Si+Al	26.03(10)	26.19(10)	26.15(8)	26.00(4)	26.05(11)	26.11(8)	26.02(9)	25.92(10)	25.89(9)	25.97(6)	25.79(9)	25.71(7)
Fe+ 0.5H	5.09(13)	5.04(13)	5.02(11)	5.19(6)	5.13(15)	5.17(8)	5.14(12)	5.41(11)	5.46(9)	5.33(12)	5.74(10)	5.77(6)
AlT ^f	0.76(10)	0.84(13)	0.86(7)	0.70(4)	0.76(11)	0.80(6)	0.74(9)	0.61(10)	0.57(10)	0.67(7)	0.37(8)	0.30(6)
FeT ^f	2.69(19)	2.69(13)	2.70(15)	2.86(7)	2.80(20)	2.80(12)	2.78(11)	3.02(9)	3.12(8)	2.92(16)	3.15(12)	3.14(7)
V[Å ³] ^g	-	739.51(21)	-	740.08(30)	-	740.43(13)	739.74(40)	-	-	739.48(50)	741.24(14)	-
H _{calc} ^h	-	2.95	-	3.03	-	2.91	3.01	-	-	3.10	3.68	-

^a oxide mixture in the molar ratio FeO:Al₂O₃:SiO₂.

^b mixture of andalusite, hercynite and wüstite on basis of the composition Fe₄Al₁₈Si_{7.5}O₄₆ with Al₂SiO₅ in excess.

^c in parentheses amount of st in %; abbreviations: and: andalusite; crn: corundum; hc: hercynite; wü: wüstite; st: staurolite; chd: chloritoid; grt: garnet; ky: kyanite; qtz: quartz

^d total iron as FeO.

^e H₂O values as determined for the single-phase Fe-staurolite syntheses (see Table 1).

^f content pfu calculated using the guidelines in Holdaway *et al.* (1991, 1995).

^g Koch-Müller *et al.* in prep.

^h H-content calculated using model B in Holdaway *et al.* (1993).

Table 2. Stoichiometry of synthetic Fe-staurolite, equilibrated at 5, 10 and 25 kbar. (1 σ : standard deviation); [σ^* : real variation] according to Holdaway *et al.* (1986b).

	5 kbar ^a	10 kbar ^b	25 kbar ^c	MKM-95-15 ^d	MKM-95-15 ^e
SiO ₂ wt %	25.22 (66)	25.91 (75)	26.41 (91)	25.04 (48)	25.01 (52)
Al ₂ O ₃ wt %	54.41 (99)	55.33 (112)	55.64(125)	55.47 (62)	55.38 (73)
FeO wt % ^f	16.53 (44)	16.04 (43)	15.33(39)	16.56 (40)	16.64 (42)
H ₂ O wt % ^g	<u>1.88(13)</u>	<u>1.65(6)</u>	<u>1.57(9)</u>	<u>1.88(6)</u>	<u>1.88(6)</u>
Σ	99.07 (88)	98.93 (109)	98.95 (107)	98.95	98.95
atoms per 48 oxygens					
Si	7.18 (17)[13]	7.39 (19)[5]	7.49 (24)[23]	7.14 (12)	7.14 (14)
Al	18.61 (25)[21]	18.56 (26)[5]	18.60 (34)[24]	18.65 (19)	18.64 (19)
Fe	3.94 (11)[2]	3.82 (11)[3]	3.64 (10)[12]	3.95 (10)	3.97 (10)
H	<u>3.58 (14)</u>	<u>3.14 (4)</u>	<u>2.97 (9)</u>	<u>3.58 (2)</u>	<u>3.59 (3)</u>
Σ	33.30 (7)	32.91 (9)	32.70 (9)	33.32 (5)	33.34 (7)
Si+Al	25.79 (10)	25.95 (10)	26.09 (11)	25.74 (4)	25.78 (8)
Fe+ 0.5H	5.73 (12)	5.39 (12)	5.12 (11)	5.74 (10)	5.77 (10)

^a Mean value of 117 analyses on 83 crystals from 4 different syntheses.

^b Mean value of 62 analyses on 49 crystals from 3 different syntheses.

^c Mean value of 85 analyses on 71 crystals from 6 different syntheses.

^d Synthesis run at 5 kbar, 680 °C; mean value of 27 analyses on 12 crystals with 10 s counting time on peak for Al and Si and 20 s for Fe.

^e Synthesis run at 5 kbar, 680 °C; mean value of 27 analyses on 15 crystals with 30 s counting time on peak for all elements.

^f total iron as FeO.

^g H₂O-values were obtained on aliquots of the bulk run products: mean values of six analyses on five run products at 5 kbar, three analyses on three run products at 10 kbar, three analyses of two run products at 25 kbar

Mg- and Zn-staurolite end-member, respectively, with water in excess.

All run products were analysed by optical microscopy, X-ray powder diffractometry and electron microprobe, some products were observed with a scanning electron microscope (SEM). The crystals were prismatic and varied in size between 2 and 10 μm lengthways and between 1 and 5 μm perpendicular to that.

Microprobe analyses

Microprobe analyses of Fe-staurolites and the additional phases were performed with a Cameca Camebax at the ZELMI laboratory of the Technische Universität Berlin, using the wavelength-dispersive mode with LiF and TAP crystals and andalusite (Al, Si) and metallic iron (Fe) as standards. Standardization and reproducibility were checked by measurements on synthetic almandine, which was present in some synthesis runs as mentioned

above. The raw data were corrected with the "PAP" program (Pouchou & Pichoir, 1985). Accelerating voltage was set at 15 kV and a beam current of 15 nA was used. Counting times were 10 s for Al and Si and 20 s for Fe with 5 or 10 s on background, respectively. Longer counting times (30 s for every element on peak and 15 s on background) were tested on one sample (MKM-95-15), but this did not improve the results. The results of the analyses in wt% are shown in Table 1 and Table 2, upper part. The relatively low totals are probably due to the well-known problems associated with the microprobe analysis of fine-grained crystals such as synthesis products. Comparison of microprobe analyses of a natural staurolite single crystal (4 \times 2 mm size) with analyses of the same staurolite, ground to a grain size of about 20–30 μm , show that the mean values of the oxides are slightly lower than those obtained on single crystal analyses, while the standard de-

viations and oxide sums for the small crystals show the same tendency as for the synthetic materials described above. However, calculated ions per formula unit for both analyses are in close agreement. Hence, we conclude that the analyses of the synthetic staurolites yield correct proportions of the components despite having somewhat low totals.

Holdaway *et al.* (1986b) describe a method to estimate the precision of staurolite analyses. Applied to our data, this method gives relative 1 σ precisions of 0.71% for Al₂O₃, 1.24% for SiO₂ and 1.99% for FeO. According to Holdaway *et al.* (1986b), the square root of the difference between the variances of the analytical data and analytical precision is a measure of the true variation in ions per formula unit for each element. This true variation is shown in brackets in Table 2.

Determination of water contents

The water contents of the bulk run products of some of the 100% Fe-staurolite powders were determined by a semimicro analytical method that combines pyrolysis in a high-frequency heating system, transport of the evolved gases by a dried gas through an oxidizing catalyst into an automatic coulometric titration system, using the so-called "Karl-Fischer" reaction. Variants of this method are well established for water determinations in minerals, rocks, glasses and ceramics (Lindner & Rudert, 1969; Turek *et al.*, 1976; Farzaneh & Troll, 1977; Westrich, 1987; Behrens, 1995). A detailed description of the apparatus and experimental procedure used here is given by Behrens (1995). As noted by Farzaneh & Troll (1977), part of the OH can be released as hydrogen from Fe²⁺-bearing samples and may not be detected in the analysis. We have used air as the carrier gas instead of argon which is commonly used for Karl-Fischer titration. Thus, hydrogen is directly oxidized at the site of its formation and reliable analyses are obtained. Tests with biotites show that the total water content of the sample is measured by this procedure.

10–30 mg of crushed staurolite were placed in a platinum crucible and introduced with a platinum sample holder into a heating chamber of the apparatus. Before starting the pyrolysis, the heating chamber was flushed with dry gas to remove traces of water which could have penetrated into the apparatus during loading or had been adsorbed onto the surface of the sample. For all staurolite samples, the amount of water adsorbed on the surface was about 0.05 wt%. This amount was sys-

tematically subtracted from the determined total water content. The temperature was raised within a few minutes from 100 to 1300 °C. The final temperature of 1300 °C was held until the end of the titration (usually 6–9 minutes). After this treatment, the sample was not molten but still showed a powdery consistency. Therefore, there is probably no undetected water retained in bubbles in the molten glass, nor any water dissolved in the glass. Experiments with synthetic phlogopite show that residual water is very low if the powders are not molten during measurements; this can be explained by the short diffusion path of water in small crystals in comparison with the relative long diffusion paths in the melt. Thus, it may be assumed that all the water has been extracted from the sample. The maximum uncertainty (2 σ) on the obtained water contents is ± 0.06 wt%. To check the method for staurolite analyses, a natural staurolite sample from Pizzo Forno (coexisting with biotite and kyanite) was analysed, yielding a water content of 2.05 ± 0.10 wt% H₂O, which corresponds well with the mean value of 1.81 wt% H₂O, analysed by Holdaway *et al.* (1986a) on three different staurolite samples from Pizzo Forno.

The H-contents of those staurolites which were grown with additional phases could not be determined by the method described above but were calculated as follows: Holdaway *et al.* (1993) expressed the unit-cell parameters of 22 natural staurolite samples as linear functions of chemical composition using multiple linear regression. They developed two models to calculate the H-content of synthetic staurolites for a given composition. Using the cation proportions and the cell volumes of the Fe-staurolites shown in Table 1, model B of Holdaway *et al.* (1993) was used to calculate the H-contents per formula unit. They agree very well with out experimentally determined H-contents on the single-phase samples (Table 1).

Infrared spectroscopy

1.3 mg of the ground synthetic staurolite powders were mixed with 450 mg KBr and pressed to discs of 13 mm diameter. The staurolite powders and the KBr were dried at 120 °C before and after the mixing to eliminate adsorbed water. Measurements were made on a Bruker IFS66 FTIR spectrometer equipped with a Global light source, a KBr beamsplitter and a DTGS detector. The operating conditions for the spectrometer were 2 cm⁻¹

resolution and 64 averaged scans. The background was measured on a blank KBr-pellet. The spectra were fitted using the program PeakFit by Jandel Scientific, (1991). The component bands were modelled by Gaussian distribution functions, according to Koch-Müller *et al.* (1995). We cannot exclude the possibility that small amounts of adsorbed water are present in the sample or in the KBr powder. However, spectra of pressed pellets of 450 mg pure KBr and of 1.5 mg quartz in 450 mg KBr indicate that the contribution of absorbed water to the spectra is less than 0.005 absorbance units.

Results and discussion

Crystal chemistry

A total of 264 analyses were carried out on Fe-staurolite phases, equilibrated at 5, 10 and 25 kbar and 680 °C. Table 2 presents the averages of the analyses, together with standard deviations 1σ . The data were recalculated on a basis of 48 oxygens; the crystal-chemical formulae are listed in the lower part of the table. Although the standard deviations are rather high in some cases, we observe a variation of the composition of Fe-staurolite with pressure. With increasing pressure, the iron content decreases from 3.94 (11) to 3.64 (10) Fe pfu and the sum of Si and Al increases from 25.79 (10) to 26.09 (11) (Si+Al) pfu. At the same time, the H-content decreases from 3.58 (14) at 5 kbar to 2.97 (9) H pfu at 25 kbar. The differences in Fe, (Al+Si) and H pfu, as seen on Table 2, are statistically significant at the 1σ level at least for the staurolites equilibrated at 5 and 25 kbar. As shown in Table 1, this variation is not a function of the different bulk composition used in the equilibrium runs to produce 100% staurolite. Irrespective of the different bulk compositions, run durations and starting materials chosen in the preliminary runs (see Table 1), the staurolites obtained at a given pressure show a distinct composition. This result was unexpected, since the activities of Al, Si and Fe²⁺ were not fixed through the coexistence of additional phases, and thus a range of staurolite compositions would generally be expected. However, this field is likely to be small, since the standard deviations of the analytical data on the synthetic staurolites are slightly higher than in the case of the natural mineral. In some synthesis runs, shown in Table 1, a mixture of andalusite, hercynite and wüstite was used with H₂O in excess to produce Fe-staurolite + garnet \pm kyanite.

In these cases, the activities of components are fixed and, thus also the composition of the staurolites so obtained. Evidence for this is provided by the lower standard deviations of the analyses. The averaged data on staurolites from such runs plot in the same fields as those obtained for the single-phase staurolites shown in Fig. 1. In one synthesis run at 10 kbar the major part of the product Fe-staurolite was crushed after a first run duration of 48 hours and then continued under the same conditions for 48 hours. The compositions of these staurolites did not change during the run prolongation, indicating that a run duration of 48 hours is sufficient to reach equilibrium conditions for staurolite.

Holdaway *et al.* (1986a) subdivided their analysed natural staurolites into two groups: those coexisting with biotite and/or garnet contain 2.7–3.4 H pfu and those which do not coexist with biotite or garnet, but instead with hemo-ilmenite, contain 4.09–4.16 H pfu. The water contents determined in this study lie in the upper part of group 1. Holdaway *et al.* (1986b) found that the stoichiometry of natural metapelitic iron-rich staurolites is characterized by (Si+Al) = 25.43 (0.13) pfu and (Fe²⁺ + Li + 0.5 H) = 5.88 (0.15). In the synthetic iron staurolites described here, Al is negatively correlated with Si (Fig. 1a), and the sums (Si+Al) and (Fe+0.5 H) are constant for a given pressure within the same e.s.d., in agreement with Holdaway *et al.* (1986b), but differ with pressure (Table 2 and Fig. 1b). It should be noted that the mean value for the stoichiometry of natural staurolites, given by Holdaway *et al.* (1986b), lies within 1 e.s.d. of the values given for the 5-kbar Fe-staurolites discussed here. The high-pressure staurolites differ from the low-pressure phases in showing an increase of (Si+Al) accompanied with a decrease of Fe pfu and H pfu. The increase of (Si+Al) pfu is mainly caused by an increase of Si, the Al-content being nearly constant. Despite the scattering of the data, it is evident that, for a constant Al-content, the 25-kbar staurolites show a higher Si-content than the 5-kbar staurolites (Table 2 and Fig. 1a). Hawthorne *et al.* (1993c) pointed out that, due to a bond-strength excess on O1, an occupancy of the H1 site must be accompanied by substitutions of low-valence cations in the “kyanite”-layer, *e.g.* Mg in M1,2 or Al in T1. This requirement is in accordance with the experimental results in the present study: the 5-kbar staurolite show a higher H1-content (as discussed below) and thus a higher Al-content in T1 than the 25-kbar staurolites. Be-

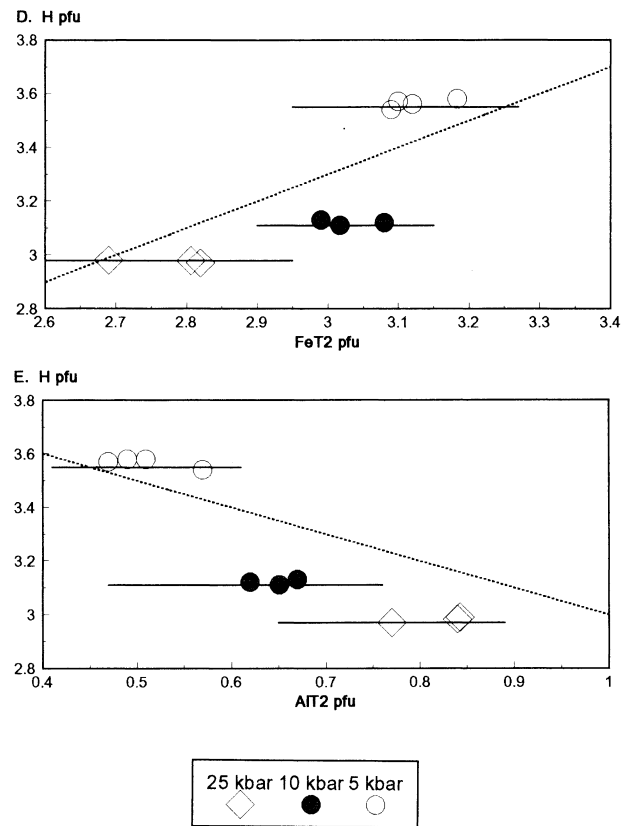
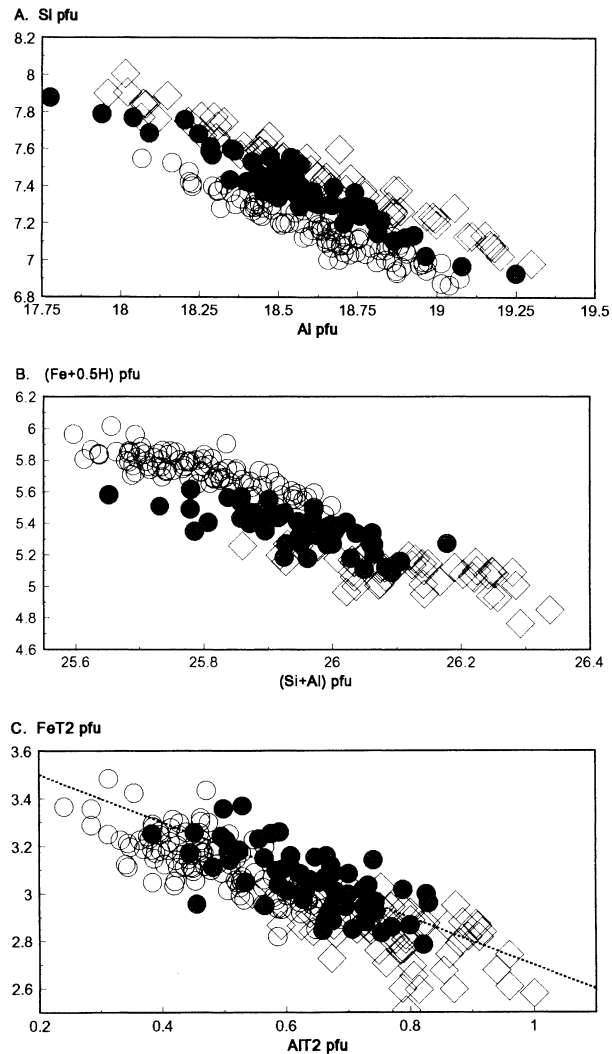


Fig. 1. Element correlations in the synthetic Fe-staurolite phases. A.: Al versus Si; B.: (Fe+0.5H) versus (Si+Al); C.: FeT2 versus AlT2, estimated using the guidelines of Holdaway *et al.* (1991); dotted line shows the ideal slope for the proposed substitution of Al for Fe²⁺ in T2; D. and E.: H versus FeT2 pfu and H versus AlT2 pfu, respectively; the data points correspond to average values for the runs with H determination.

Table 3. Si, Al, Fe²⁺ end-member compositions (atoms pfu) of natural (Holdaway *et al.*, 1991) and of synthetic staurolite of this study, as calculated according to procedure of Holdaway *et al.* (1991, 1995).

		after Holdaway <i>et al.</i> , 1991		Fe-staurolite 5 kbar	Fe-staurolite 10 kbar	Fe-staurolite 25 kbar
M1	Al	7.70	} 8	7.70	7.70	7.70
	Fe	0.30		0.30	0.30	0.30
M2	Al	7.80	} 8	7.80	7.80	7.80
	Fe	0.20		0.20	0.20	0.20
M3	Al	1.81	} 2	1.80	1.82	1.80
	Fe	0.12		0.12	0.12	0.12
	□	0.07		0.08	0.06	0.08
M4	Fe	0.18	} 4	0.20	0.17	0.20
	□	3.82		3.80	3.83	3.80
T1	Si	7.64	} 8	7.18	7.39	7.49
	Al	0.36		0.82	0.61	0.51
T2	Fe	3.40	} 4	3.12	3.03	2.82
	Al	0.24		0.49	0.63	0.79
	□	0.36		0.39	0.34	0.39

cause of the constant Al-content, an increase in Si must be accompanied by an increase of Al in sites other than T1, *e.g.* (Al^{10L}–(8–Si)) pfu (note that this amount is equal to ((Si+Al)–8)). Holdaway *et al.* (1991 and 1995) give guidelines to recast chemical analyses of staurolite in terms of site occupancies. These guidelines are based on the study of Hawthorne *et al.* (1993a), who investigated 42 natural staurolites by single-crystal four-circle diffractometry. Holdaway *et al.* (1991, 1995) followed an approach involving almost constant Al-contents in M1, M2 and M3. This approach is suitable to estimate the site population of T2 by Fe, Al and vacancies (□). Table 3 shows a comparison of the calculated Si, Al, Fe²⁺ end-member composition given by Holdaway *et al.* (1991) with the compositions calculated in the present study using the guidelines cited above. From this, it is clear, that the increase in (Al^{10L}–(8–Si)) with pressure is caused by an increase of Al in T2 (AlT2) accompanied by a decrease of Fe in T2 (FeT2) whereas vacancies in T2 remain almost constant (Fig. 1c). This tendency is also seen in all the staurolites shown in Table 1. We conclude, that in the synthetic staurolites discussed here substitution of Fe²⁺ by Al³⁺ in T2 is induced by raising pressure, consistent with the fact that Al³⁺ is smaller than Fe²⁺. The dominance of this substitution can be seen in a plot of AlT2 *versus* Fe²⁺T2, which shows a slope of –1 (Fig. 1c). This substitution increases the net positive charge in the stau-

rolites and must, thus, be coupled with charge reducing substitutions (Hawthorne *et al.*, 1993c). Hawthorne *et al.* (1993c) give three possible exchange vectors (7 to 9) involving Al incorporation in T2 plus the charge compensation needed, which can be summarized here as:

- (i) [Al^{T2}□_{0.5}^{M3}H_{0.5}]₁[Fe²⁺T2Al_{0.5}^{M3}□_{0.5}H]_{–1} (exchange vector 7)
- (ii) [Al^{T2}Al^{T1}]₁[Fe²⁺T2Si^{T1}]_{–1} (exchange vector 8)
- (iii) [Al^{T2}Mg^{M1,2}]₁[Fe²⁺T2Al^{M1,2}]_{–1} (exchange vector 9)

On the basis of observations in the present study, we can add a fourth exchange vector:

- (iv) [Al^{T2}□^{H1}]₁[Fe²⁺T2H^{H1}]_{–1}.

The further exchange vectors

- (v) [Fe²⁺T2H^{H1}Al^{T1}]₁[Fe²⁺T2Si^{T1}]_{–1}
- (vi) [Al^{T2}H^{H1}Al^{T1}]₁[Al^{T2}Si^{T1}]_{–1}

are introduced to account for a high excess bond strength on O1 in case of H1 occupancy.

Exchange vector (i) may be active in the synthetic staurolites, but is difficult to detect. Calculations of Si, Al, Fe end-member compositions do not indicate a raising vacancy concentration in M3 with increasing pressure. Exchange vector (ii) is not in accordance with the present experimental results: Si-contents pfu increase with increasing

AIT2. Exchange vector (iii) (using Fe^{2+} instead of Mg) could be applicable, but would not reduce the total amount of Fe^{2+} with increasing AIT2 as observed in the synthetic staurolites. Exchange vector (iv) implies a linear correlation of H1 pfu versus AIT2 and H1 pfu versus $\text{Fe}^{2+}\text{T2}$ with slopes of -1 and 1 , respectively. The proton site involved in this exchange vector is the H1 site since the H2 and H3 sites are only occupied if T2 is vacant. Figures 1d and e demonstrate that the experimental results, using the total H-content, are close to the theoretical slopes (dotted lines), but probably do not fit the linear correlations. Exchange vectors (v) and (vi) describe the observed increase of Si and decrease of H with pressure, but do not account for the strong correlation of AIT2 with $\text{Fe}^{2+}\text{T2}$.

In summary, none of these charge-reducing substitutions, represented by exchange vectors (i) to (vi), is likely to be the only one able to explain the pressure induced incorporation of Al in T2. To explain the correlations, shown in Figures 1c, d, and e, it should be borne in mind that the calculated amounts of $\text{Fe}^{2+}\text{T2}$ and AIT2 are based on the assumption of a constant value of 0.62 Fe^{2+} pfu in M1–M3 (Holdaway *et al.*, 1991). In principle, however, exchange vector (iii) implies variable amounts of Fe^{2+} in M1 and M2, whereby increasing amounts would involve a decrease in $\text{Fe}^{2+}\text{T2}$ and connected increase in AIT2 and *vice versa* in the case of falling $\text{Fe}^{2+}(\text{M1}, \text{M2})$. Such operations would not affect the correlation shown in Fig. 1c. However, they would produce a larger scatter in the correlations in Figures 1d and e with the same trend as observed (increasing AIT2 \Rightarrow decreasing $\text{Fe}^{2+}\text{T2}$). In addition, in Figures 1d and e the total H-content of staurolite is used instead of the H1-content. The infrared spectra shown in the next section, however, indicate that the H-content in the H2 site increases with pressure and this may also cause the deviation of the experimental data from the ideal slope in Figures 1d and e. Thus, the element correlations shown in Figures 1c, d and e can be interpreted as being caused by a combination of the exchange vectors (i) to (vi), while ruling out (ii). The compositional variations of the synthetic staurolites reported here may thus be described by an increasing substitution of Fe^{2+} through Al in T2 with increasing pressure – the charge balance being maintained by vacancies in the proton sites H1 and/or M3 site (exchange vector (i) and (iv)), Al substitution for Si in T1 (exchange vector (v) and (vi)) and by a substitu-

tion of Al through Fe^{2+} in the M1 and M2 sites (exchange vector (iii)). However, the existence of exchange vector (iii) is difficult to establish because the amount of Fe^{2+} pfu necessary to produce the observed deviation from the ideal slope for exchange vector (iv) is very small (about 0.1 pfu). Results of Mössbauer spectroscopy, performed on synthetic Fe-staurolites equilibrated at 25 and 5 kbar (Koch-Müller & Abs-Wurbach, 1996), agree well with the occupancies calculated for T2 obtained in the present study; however, changes in M1–M4 occupancies with pressure could not be detected.

Lattard & Bubenik (1995) synthesized staurolites in the system Mg-Fe-Al-Si-O-H at 20 kbar and temperatures between 720 and 800 °C. The composition and molar volume of their Fe-staurolites (WM buffer) agree very well with the data of the 25-kbar staurolites in the present study.

Fockenbergl (1995) investigated the crystal chemistry of Mg-staurolites in the pressure range 20–50 kbar. Over the whole pressure range, he used a gel as starting material having the oxide ratio $4 \text{ MgO} : 9 \text{ Al}_2\text{O}_3 : 8 \text{ SiO}_2$ to produce 100% Mg-staurolite plus traces of corundum. He found that H pfu increases from 2.45 at 20 kbar to 3.92 at 50 kbar and that the Mg-content increases in the pressure range 20–30 kbar from 3.78 to 4.08 pfu and decreases in the pressure range 30–50 kbar from 4.08 to 3.71 pfu, while the Al-content decreases over the whole pressure range. The crystal chemical formula for the Mg-staurolite, synthesized at 25 kbar and 800 °C is given as $\text{Mg}_{3.90}\text{Al}_{18.04}\text{Si}_{7.78}\text{O}_{45.06}(\text{OH})_{2.94}$, which agrees well with the formula obtained for the Fe-staurolite equilibrated at 25 kbar in the present study, especially with respect to the H-content (see Table 2). However, the crystal chemical variation of the Mg-staurolite with pressure as observed by Fockenbergl (1995) cannot be compared with the present results because of the different pressure ranges investigated. At higher pressures, additional substitution mechanisms may occur. In addition, the crystal chemistry of the Mg-staurolites differs from that of the Fe-staurolites in having a higher amount of Mg in M4, leading to a decrease in MgT2 and an increase in H (Fockenbergl, 1995; Hawthorne *et al.*, 1993a,c).

The decrease of M^{2+} with pressure observed in the present study is in accordance with the results of Holdaway *et al.* (1995) on natural staurolite. Yet, these authors observe an increase of H pfu with increasing pressure for staurolites coexisting

either with Al-silicate plus quartz or garnet plus quartz for example about 4.2 H pfu at 13 kbar and 650 °C). Holdaway *et al.* (1995) argue that synthetic staurolites could have low H-content due to the use of bulk compositions which differ from the equilibrium composition of the staurolites. The staurolites in the present study, however, show a distinct composition at a given pressure irrespective of the different bulk compositions used (see syntheses conditions) and there is no indication of increasing H-contents in pure Fe-staurolite with pressure.

Infrared spectroscopy

The IR powder spectra of synthetic staurolite in the range of 3000–4000 cm^{-1} are compared here with unpolarized single crystal spectra of a natural staurolite from Pizzo Forno which has been measured and assigned by Koch-Müller *et al.* (1995). These authors modelled the component bands by Gaussian distribution functions and classified the observed bands into three groups according to their polarization behaviour:

- Group I contains a strong band at 3445 cm^{-1} which can be resolved into two component bands ν_{H1B} at 3468 cm^{-1} and ν_{H1A} at 3424 cm^{-1} plus a shoulder ν_{H1cpd} at 3358 cm^{-1} .
- Group II contains a weak band ν_{H2I} at 3677 cm^{-1} plus a shoulder ν_{H2II} at 3635 cm^{-1} .
- Group III contains a weak band ν_{H3I} at 3577 cm^{-1} plus a shoulder ν_{H3II} at 3525 cm^{-1} .

The protons H1–H3 in the staurolite structure (Koch-Müller *et al.*, 1995) are all bonded to O1A or O1B oxygens. These oxygens are coordinated by two M2 sites, one T2 site, the M4A or (M4B) and the M3A or (M3B) sites. In this arrangement, only the M2 sites are completely filled. The other sites show more or less pronounced vacancies. The shoulders in groups II and III are suggested by Koch-Müller *et al.* (1995) to be caused by Fe^{2+} substitution in M2.

A precise analysis of IR spectra of synthetic staurolite phases was expected to yield information on the site occupancy of the coordinating sites M2, T2, M4 and M3. The relatively high scatter in Si and Al in T1 of the staurolites is not expected to influence the IR spectra since the corresponding T1 site is not a near neighbour of the OH-dipole. Fig. 2 shows the IR powder spectra of Fe-, Mg- and Zn-staurolite phases synthesized at 25 kbar. All three band groups mentioned above can

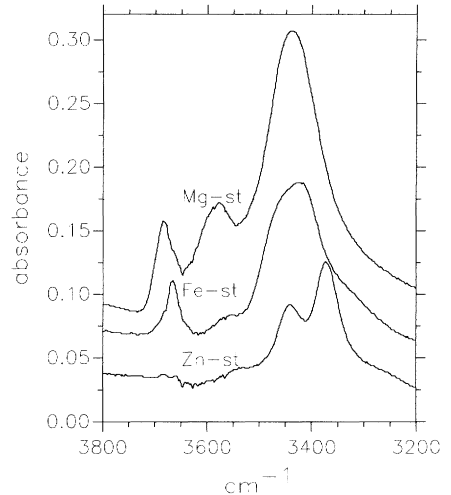


Fig. 2. Infrared spectra of synthetic Fe-, Mg- and Zn-staurolite.

be observed in the Fe- and Mg-staurolite spectra. Spectra bands belonging to group II are absent in the Zn-staurolite.

Fe-staurolite

Fig. 3 compares the room-temperature spectrum of Fe-staurolite synthesized at 25 kbar with the one recorded on the same sample at 77 K. The spectrum clearly supports the assignment of band ν_{H3} to be a vibration of hydroxyl groups rather than of water inclusions in the staurolites (see Koch-Müller *et al.*, 1995). Fig. 4 shows the room-temperature spectra of Fe-staurolites equilibrated at different pressures. These staurolites differ not only in their crystal chemistry (Table 2) but also in their IR-spectra.

As pointed out by Koch-Müller *et al.* (1995), the main band at 3345 cm^{-1} present in the spectrum of natural staurolite of Pizzo Forno was decomposed into two component bands only. In this simplified model, one band results from vibration of an O1-H1A dipole, the other from vibrations of an O1-H1B dipole with a broad halfwidth, because the OH-coordinating T2 site can be occupied by several different cations (Fe,Mg,Zn,Mn,Al). In the synthetic Fe-staurolite there is only Fe and Al in T2. Therefore, a lower halfwidth of the $\nu_{\text{H1A,B}}$ bands is to be expected. Fig. 5a shows a fit of the 5-kbar Fe-staurolite using a lower halfwidth than in the natural stauo-

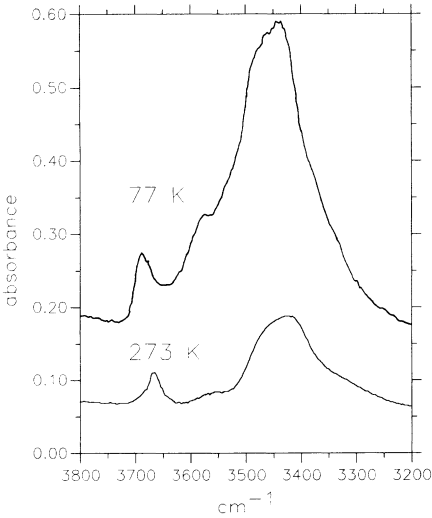


Fig. 3. Infrared spectra of synthetic Fe-staurolite, equilibrated at 25 kbar, recorded at room temperature and at 77 K.

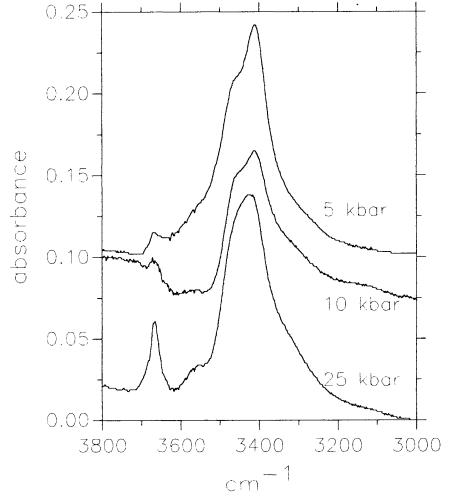


Fig. 4. Infrared spectra of synthetic Fe-staurolite, equilibrated at different pressures.

lite and, in addition to the bands described above, two component bands which we relate to Al in T2, (*i.e.* ν_{HIBA1} and ν_{HIAA1}). The corresponding data of the component bands are summarized in Table 4. In comparison to the natural staurolite from Pizzo Forno, some of the component bands are found to be shifted to lower wavenumbers by about 20 cm^{-1} . Since real absorbancies cannot be obtained from KBr-powder spectra, relative absorbance values

$$(A_{\text{rel. } i} = A_i / \sum_{i=1}^k A_i)$$

are given in Table 4. As discussed above, the differences in crystal chemistry of the Fe-staurolites equilibrated at 5, 10 and 25 kbar are chiefly characterized by an increase of the Al-content in T2 with pressure. In agreement with this, Fig. 5b shows that the fitted spectrum for the 25-kbar staurolite contains the ν_{HIAA1} band with a higher relative absorbancy than the 5-kbar staurolite spectra. Due to the decreasing water content of staurolite with pressure, the relative absorbancies are, however, not a suitable measure for comparing the intensity differences of the ν_{HIAA1} bands. A criterion for intensity differences of the ν_{HIAA1} bands is, however, the ratio between the absorbancies of the ν_{HIA} plus ν_{HIB} bands and the absorbancy of the ν_{HIAA1} band. The ratio decreases with pressure from 21.60 for the 5-kbar spectra to

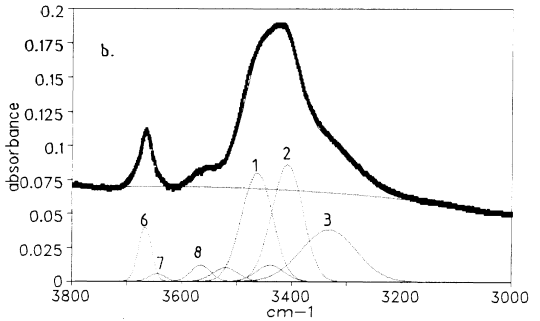
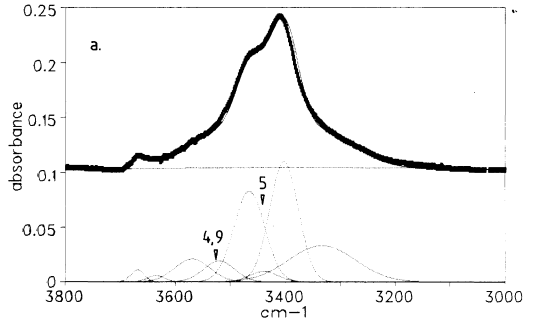


Fig. 5. a.: Experimental and fitted spectrum of synthetic Fe-staurolite, equilibrated at 5 kbar. For labels of the bands, see also Fig. 5b. The nomenclature of the bands is given in Table 4.

b.: Experimental and fitted spectrum of synthetic Fe-staurolite, equilibrated at 25 kbar.

Table 4. Peakfit results of the IR-spectra in the ν_{OH} -vibrational range.

	Fe-staurolite (25 kbar) $r^2=0.997$			Fe-staurolite (10 kbar) $r^2=0.996$			Fe-staurolite (5 kbar) $r^2=0.996$			Mg-staurolite (25 kbar) $r^2=0.996$			Zn-staurolite (25 kbar) $r^2=0.996$		
	cm ⁻¹	relative absorbance ^d	half width cm ⁻¹	cm ⁻¹	relative absorbance ^d	half width cm ⁻¹	cm ⁻¹	relative absorbance ^d	half width cm ⁻¹	cm ⁻¹	relative absorbance ^d	half width cm ⁻¹	cm ⁻¹	relative absorbance ^d	half width cm ⁻¹
group I ^c															
ν_{H1B} (1)	3466	0.273	66	3465	0.188	66	3469	0.185	64	3466	0.199	82	3440	0.194	59
ν_{H1A} (2)	3409	0.273	66	3406	0.243	68	3405	0.247	66	3412	0.193	82	3370	0.293	54
ν_{H1A1B} ^a	3427	0.321	128	3429	0.334	136	3429	0.369	143	3436	0.302	100	3405	0.362	142
ν_{H1end} ^b (3)	3333	0.130	118	3330	0.100	118	3333	0.073	141	3325	0.063	141	3295	0.086	141
ν_{H1BA1} (4)	3520	0.043 ^c	54	3519	0.024 ^c	47	3520	0.042 ^c	66	-	-	-	-	-	-
ν_{H1AA1} (5)	3439	0.040	59	3439	0.021	59	3439	0.020	59	-	-	-	-	-	-
group II ^c															
ν_{I2I} (6)	3668	0.133	28	3668	0.030	28	3668	0.022	28	3675	0.068	32	-	-	-
ν_{I2II} (7)	3645	0.020	28	3645	0.012	35	3635	0.013	35	3695	0.045	28	-	-	-
group III ^c															
ν_{I3I} (8)	3565	0.043	42	3565	0.021	42	3569	0.046	75	3570	0.098	75	3534	0.039	71
ν_{I3II} (9)	3520	0.043 ^c	42	3519	0.024 ^c	47	3520	0.042 ^c	66	3618	0.033	71	3483	0.026	71

^a ν_{H1AB} denotes the unresolved band due to H1 protons.^b ν_{H1end} denotes the additional band at the low energy side possibly due to coupling of frequencies.^c ν_{H1BA1} and ν_{I3II} overlap, so the absorbance is given for the resulting band.^d relative absorbance $A_{\text{rel},i} = A_i / \sum_{i=1}^k A_i$.^c numbers in parentheses refer to labels in Figures 5a, b.

13.65 for the 25-kbar spectra indicating increasing intensity of the ν_{H1AA1} bands with increasing pressure. This should also be reflected in the intensity of the ν_{H1BA1} band, but the intensities of the ν_{H1BA1} bands in the spectra of both staurolites cannot be compared due to overlapping with the ν_{H3II} bands. Thus, the difference in the IR-spectra of Fe-staurolite synthesized at 5 and at 25 kbar may reflect the pressure-induced substitution of Fe^{2+} through Al in T2. The fact that $\nu_{\text{H1A.BA1}}$ bands exist in the spectra supports the hypothesis that exchange vector (iv) is not the exclusive charge-reducing mechanism in the synthetic staurolites but should be combined with exchange vectors (i) and (vi). Differences in the intensities of ν_{H2} between the 25- and 5-kbar staurolites may result indirectly from the exchange vector (iv). At 25 kbar, the H1 site is less occupied due to incorporation of Al^{3+} in T2. This may cause a higher population in H2, although the total H-content at 25 kbar is lower compared to 5 kbar.

Mg-staurolite

Fig. 6 shows the result of a Gaussian fit for the IR-spectrum of Mg-staurolite synthesized at 25 kbar. In Table 4, the corresponding data of the band fit is compared with the data of the Fe-staurolite synthesized at 25 kbar. The main difference between these two spectra is the position for the bands ν_{H2II} and ν_{H3IF} . These bands are interpreted in natural staurolite to be caused by incorporation of Fe instead of Al into M2 (Koch-Müller *et al.*, 1995). In Mg-staurolite, these bands should either be absent (only Al in M2) or occur at higher wavenumbers due to Mg incorporation in M2. Fig. 6

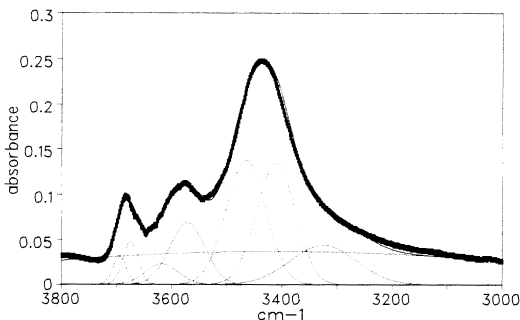


Fig. 6. Experimental and fitted spectrum of synthetic Mg-staurolite.

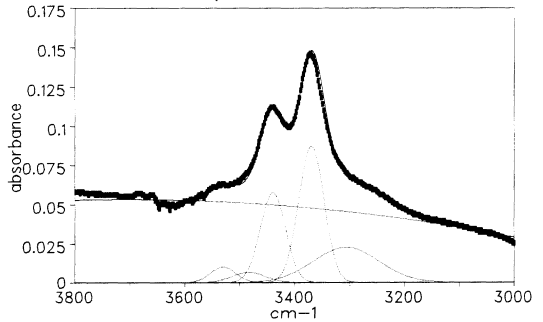


Fig. 7. Experimental and fitted spectrum of synthetic Zn-staurolite.

shows a fit of the spectrum with shoulders at the high-energy side of the bands ν_{H2} and ν_{H3} , indicating Mg incorporation in M2. There is no evidence of Al in T2 in the Mg-staurolite phase (Hawthorne *et al.*, 1993a), so, no bands for Al in T2 can be fitted into the main band.

Zn-staurolite

Fig. 7 shows the result of a Gaussian fit of the IR-spectrum of Zn-staurolite synthesized at 25 kbar. The corresponding data are summarized in Table 4. All bands are shifted to lower wavenumbers and the difference in energy between ν_{H1A} and ν_{H1B} is higher than observed in the spectra of Mg- and Fe-staurolites, so these two bands occur as distinct bands in Zn-staurolite. The shoulder ν_{H3II} is interpreted as being due to Zn incorporation in M2. However, it is not possible to fit additional bands for Al in T2 under the envelope of the main bands. This is in accordance with the structure refinement of a Zn-rich natural staurolite given by Hawthorne *et al.* (1993a). Low Al-content in T2 implies a higher Zn concentration when compared to the respective population in the Fe-staurolite synthesized at 25 kbar. This conclusion is supported by the synthesis results at 25 kbar, where a mixture of composition $\text{Zn}_4\text{Al}_{18}\text{Si}_{7.5}\text{O}_{46}$ produced a yield of 100%. Preliminary microprobe analyses of Zn-staurolites (Bubenik, pers. comm.) suggest higher occupation of Zn in T2, therefore less Al and less vacancies. The band at about 3668 cm^{-1} , which is due to O-H2 vibrations, is absent in the Zn-staurolite spectrum, showing that there are no configurations involving H2. This observation indicates that Zn-staurolites synthesized at 25 kbar contain lower vacancy concentrations in T2 than

Fe-staurolite synthesized under the same pressure, since occupation of H2 is correlated with vacancies in T2.

Discussion of site assignments

Koch-Müller *et al.* (1995) clearly showed that the bands of groups I, II and III are related to H1, 2 and 3 and that the main bands $\nu_{\text{H1A,B}}$, ν_{H2I} , ν_{H3I} are related to the "normal" configuration in staurolite with Al in M2, Fe^{2+} or \square in T2, \square or Al in the adjacent M3 sites and \square in the adjacent M4 sites. The restricted number of elements in the synthetic staurolites makes it possible to use the IR-spectra to obtain further insight on the substitution mechanisms and local arrangements around the O1 oxygen.

The energy of an OH-band is strongly anticorrelated with the electronegativity of the cations bonded to the hydroxyl ions (Bancroft *et al.*, 1966; Strens, 1974; Hawthorne, 1981). These authors propose a negative correlation even for heterovalent substitutions where the aggregate bond-valence on the hydroxyl oxygen is changed. On the other hand, increasing aggregate bond-valence on oxygens of OH groups decreases the energy of the corresponding bands. In amphiboles, for example,

the effect of bond-valence on the hydroxyl oxygen is thought to be much stronger than the effect due to the electronegativity differences between the cations (Della Ventura, pers. comm.). Robert *et al.* (1989) investigated the relationship between OH-stretching wavenumbers and composition of synthetic solid solutions between phlogopite (Mg_3) and each of the end-members taeniolite (Mg_2Li), trillithionite ($\text{Al}_{1.5}\text{Li}_{1.5}$) and polyolithionite (Li_2Al), where the OH coordinating sites are given in parentheses. They observed a decrease in the wavenumber of ν_{OH} with increasing aggregate bond-valence. However, increasing bond-valence is here also accompanied by an increase in the mean electronegativity of the cations bonded to the hydroxyl ions. Thus, in heterovalent substitutions, such as Fe^{2+} substitution for Al in the octahedral M2 site of staurolite (where the mean electronegativity increases from 1.47 to 1.56 and the aggregate bond-valence on O1 decreases from 1.00 to 0.83 v.u.) it is an open question which quantity has stronger influence, electronegativity or aggregate bond-valence.

Hawthorne *et al.* (1993c) compiled all possible arrangements in staurolite around the O1A and B oxygens and evaluated the relative probability of these arrangements. Table 5 gives a compila-

Table 5. Cation configurations, aggregate bond-valences and mean electronegativities around O1A in Fe- and Mg-staurolite by occupation of H1A and H2A.

protons	local arrangement ^a	cations ^b	cation configuration around OH ^b	Pauling bond-valence on O1A ^c	mean electronegativity ^d
H2 A	2 M2 occupied M4A vacant M3A vacant T2 vacant M4B occupied	Al, M	$\square \text{T}^2\text{Al}^{\text{M}2}\text{Al}^{\text{M}2}$	1.00	1.47
			$\square \text{T}^2\text{Al}^{\text{M}2}\text{Al}^{\text{M}2}$	0.83	1.56 (M = Fe^{2+}) 1.35 (M = Mg)
H1 A	2 M2 occupied T2 occupied M3A vacant M4A vacant M4B vacant	Al, M	$\text{M}^{\text{T}2}\text{Al}^{\text{M}2}\text{Al}^{\text{M}2}$	1.50 ^e	1.53 (M = Fe^{2+}) 1.39 (M = Mg)
			M, Al	$\text{Al}^{\text{T}2}\text{Al}^{\text{M}2}\text{Al}^{\text{M}2}$	1.75 ^e
		$\text{Al}^{\text{T}2}\text{Al}^{\text{M}2}\text{M}^{\text{M}2}$		1.58 ^e	1.53 (M = Fe^{2+}) 1.39 (M = Mg)
		$\text{M}^{\text{T}2}\text{Al}^{\text{M}2}\text{M}^{\text{M}2}$	1.33 ^e	1.58 (M = Fe^{2+}) 1.31 (M = Mg)	

^a most probable configurations according to Hawthorne *et al.* (1993c).

^b M = Fe^{2+} in Fe-staurolite and Mg in Mg-staurolite.

^c bond-valence calculated by dividing cationic charge by the coordination number.

^d Allred-Rochow electronegativities.

^e As discussed by Hawthorne *et al.* (1993c) these high excess bond-strengths on O1 should be compensated by charge-reducing substitutions in the "kyanite"-layer, e.g. Al substitution for Si in T1 or Fe, Mg substitution for Al in M1,2.

tion of the most probable arrangements for Fe- and Mg-staurolites, the possible substitution mechanisms, resulting mean electronegativities and aggregate bond-valences. In the Fe- and Mg-staurolite phases only three cation configurations around H2A are possible (excluding the improbable configuration that both M2 sites are occupied by M^{2+}):

- (i) $\square T^2Al^{M2}Al^{M2}$
- (ii) $\square T^2Al^{M2}Fe^{M2}$
- (iii) $\square T^2Al^{M2}Mg^{M2}$.

Configuration (i) is related to the ν_{H2I} bands in both the Fe- and Mg-staurolites. Configuration (ii) and (iii) have equal aggregate bond-valence, which is lower than that observed for configuration (i), while the mean electronegativity is lower in configuration (ii) and higher in configuration (iii) (Table 5). Since the spectra of the synthetic Fe- or Mg-staurolites clearly show a shoulder either at the low- or at the high-energy side, respectively, of the ν_{H2I} band, we assume that the respective shoulder corresponds to configuration (ii) in the case of Fe-staurolite and to configuration (iii) in the case of Mg-staurolite. The observed pleochroic behaviour of the ν_{H2I} band and shoulders just mentioned (Koch-Müller *et al.*, 1995) indicate that they are caused by vibrations of the O-H2 dipole. In addition, the local arrangement around O-H2 of Table 5 is the only one which could explain these shoulders since the adjacent sites are vacant. Thus, we propose that increasing mean electronegativities in a given local arrangement in staurolite have a higher influence on the OH-vibrational energies than changes in the aggregate bond-valences.

The most probable configurations around H1A are:

- (i) $Fe^{2+}T^2Al^{M2}Al^{M2}$ and (ii) $Mg^{T2}Al^{M2}Al^{M2}$ the "normal" arrangement in staurolite
- (iii) $Al^{T2}Al^{M2}Al^{M2}$
- (iv) $Al^{T2}Al^{M2}Fe^{2+M2}$ and (v) $Al^{T2}Al^{M2}Mg^{M2}$
- (vi) $Fe^{2+T2}Al^{M2}Fe^{M2}$ and (vii) $Mg^{T2}Al^{M2}Mg^{M2}$

Following above discussion, we expect the OH-vibrational bands in configuration (iii) at higher wavenumbers than the bands in configuration (i). Arrangements (iv) and (v) have a very low probability. The corresponding bands may, thus, be hidden in the envelope of the spectra. Due to the high mean electronegativity, configuration (vi) in Fe-staurolite (and configuration $Zn^{T2}Al^{M2}Zn^{M2}$ in Zn-staurolite; mean electronegativity: 1.62) can

be assigned to the band with the lowest wavenumber, *i.e.* the ν_{H1cpd} band whose site assignment has not been elucidated in previous work (Koch-Müller *et al.*, 1995). However, since band ν_{H1cpd} occurs also in Mg-staurolite at a very low wavenumber and since the corresponding $Mg^{T2}Al^{M2}Mg^{M2}$ configuration exhibits a mean electronegativity of 1.31, this assignment remains questionable.

Conclusions

The results of microprobe analyses, water-content determinations and infrared spectroscopy on synthetic staurolites show that:

- (i) Fe-staurolites synthesized at different pressures differ in their crystal chemistry: with increasing pressure, the total iron content decreases from 3.94 at 5 kbar to 3.64 Fe pfu at 25 kbar and AlT2, calculated after Holdaway *et al.* (1991, 1995), increases from 0.49 to 0.79 pfu. Concomitantly, the H-content decreases from 3.58 to 2.97 H pfu.
- (ii) To explain results on Fe-staurolite, a heterovalent substitution of Fe^{2+} through Al^{3+} in T2 is suggested. With increasing pressure this implies that the smaller Al substitutes for Fe^{2+} in T2, the charge balance being maintained by vacancies in the proton sites and the M3 site, along with Al substitution in T1 and Fe^{2+} substitution in M1,2. The proposed substitution is corroborated by the ν_{OH} -spectra.
- (iii) The ν_{OH} -spectra indicate that there is a significant amount of Fe^{2+} , Mg and Zn in the M2 sites of the corresponding phases.

Acknowledgements: We would like to thank H. Reuff for careful preparation of the microprobe samples and F. Galbert at ZELMI for help in the microprobe work. Thanks are also due to H. Winkelmann for preparing parts of the high-pressure equipment and to S. Freitag for measuring some of the infrared spectra. D. Lattard and W. Bubenik are thanked for helpful discussions and comments. We thank the editors and reviewers Th. Armbruster (Bern), G. Della Ventura (Roma), B. Dutrow (Baton Rouge), M. Holdaway (Dallas), E. Libowitzky (Pasadena, Bern) and W. Maresch (Münster) for constructive and helpful suggestions on early versions of the manuscript which have led to substantial improvements. This project was supported by a grant from the Deutsche Forschungsgemeinschaft under the number Ko1260/1.

References

- Alexander, V.D. (1989): Iron distribution in staurolite at room and low temperatures. *Am. Mineral.*, **74**, 610–619.
- Bancroft, G.M., Burns, R.G., Strens, R.G.J. (1966): Cation distribution in anthophyllite from Mössbauer and infrared spectroscopy. *Nature*, **212**, 913–915.
- Behrens, H. (1995): Determination of water solubilities in high-viscosity melts: An experimental study on $\text{NaAlSi}_3\text{O}_8$ and KAlSi_3O_8 melts. *Eur. J. Mineral.*, **7**, 705–920.
- Cemic, L., Geiger, C.A., Hoyer, W., Koch-Müller, M., Langer, K. (1990): Piston-cylinder techniques: Pressure and temperature calibration of a pyrophyllite-based assembly by means of DTA measurements, a salt-based assembly and a cold sealing sample encapsulation method. *N. Jb. Mineral. Mh.*, **1990**, 49–64.
- Dutrow, B.L. (1991): The effects of Al and vacancies on Li substitution in iron staurolite: a syntheses approach. *Am. Mineral.*, **76**, 42–48.
- Dyar, M.D., Perry, C.L., Rebbert, C.R., Dutrow, B.L., Holdaway, M.J., Lang, H.M. (1991): Mössbauer spectroscopy of synthetic and naturally occurring staurolite. *Am. Mineral.*, **76**, 27–41.
- Farzaneh, A. & Troll, G. (1977): Quantitative Hydroxyl- und H_2O -Bestimmungsmethode für Minerale, Gesteine und andere Festkörper. *Fresenius Z. anal. Chem.*, **287**, 43–45.
- Fockenbergh, T. (1995): Synthesis and chemical variability of Mg-staurolite in the system $\text{MgO-Al}_2\text{O}_3\text{-SiO}_2\text{-H}_2\text{O}$ as a function of water pressure. *Eur. J. Mineral.*, **7**, 1373–1381.
- Griffen, D. (1981): Synthetic Fe/Zn staurolites and the ionic radius of $^{19}\text{Zn}^{2+}$. *Am. Mineral.*, **66**, 932–937.
- Hawthorne, F.C. (1981): Amphibole spectroscopy. *Reviews in Mineral.*, **9 A**, 103–136.
- Hawthorne, F.C., Ungaretti, L., Oberti, R., Caucia, F., Callegari, A. (1993a): The crystal chemistry of staurolite. I. Crystal structure and site populations. *Can. Mineral.*, **31**, 551–582.
- (1993b): The crystal chemistry of staurolite. II. The orthorhombic \Rightarrow monoclinic phase transition. *Can. Mineral.*, **31**, 583–595.
- (1993c): The crystal chemistry of staurolite. III. Local order and chemical composition. *Can. Mineral.*, **31**, 597–616.
- Holdaway, M.J., Dutrow, B.L., Borthwick, J., Shore, P., Harmon, R.S., Hinton, R.W. (1986a): H content of staurolite as determined by H extraction line and ion microprobe. *Am. Mineral.*, **71**, 1135–1141.
- Holdaway, M.J., Dutrow, B.L., Shore, P. (1986b): A model for the crystal chemistry of staurolite. *Am. Mineral.*, **71**, 1142–1159.
- Holdaway, M.J., Gunst, R.F., Mukhopadhyay, B., Dyar, M.D. (1993): Staurolite end-member molar volumes determined from unit-cell measurements of natural specimens. *Am. Mineral.*, **78**, 56–67.
- Holdaway, M.J., Mukhopadhyay, B., Dutrow, B.L. (1995): Thermodynamic properties of stoichiometric staurolite $\text{H}_2\text{Fe}_4\text{Al}_{18}\text{Si}_8\text{O}_{48}$ and $\text{H}_6\text{Fe}_2\text{Al}_{18}\text{Si}_8\text{O}_{48}$. *Am. Mineral.*, **80**, 520–533.
- Holdaway, M.J., Mukhopadhyay, B., Dyar, M.D., Rumble III, D., Grambling, J.A. (1991): A new perspective on staurolite crystal chemistry: Use of stoichiometric and chemical end-members for a mole fraction model. *Am. Mineral.*, **76**, 1910–1919.
- Koch-Müller, M. & Abs-Wurbach, I. (1996): Crystal-chemistry of synthetic Fe-Mg staurolite, investigated by Mössbauer-Spectroscopy. *Phys. Chem. Minerals*, **23**, 239–240.
- Koch-Müller, M., Langer, K., Beran, A. (1995): Polarized single-crystal FTIR-spectra of natural staurolite. *Phys. Chem. Minerals*, **22**, 108–114.
- Lattard, D. & Bubenik, W. (1995): Synthetic staurolites in the system Mg-Fe-Al-Si-O-H. *Eur. J. Mineral.*, **7**, 931–947.
- Lindner, B. & Rudert, V. (1969): Eine verbesserte Methode zur Bestimmung des gebundenen Wassers in Gesteinen, Mineralen und anderen Festkörpern. *Z. Anal. Chem.*, **248**, 21–24.
- Lonker, S.W. (1983): The hydroxyl content of staurolite. *Contrib. Mineral. Petrol.*, **84**, 36–42.
- Phillips, L.V. & Griffen, D.T. (1986): Staurolite-lusakite series. I. Synthetic Fe-Co staurolites. *Am. Mineral.*, **71**, 1461–1465.
- Pouchou, J.L. & Pichoir, F. (1985): "PAP" Φ (ρZ) procedure for improved quantitative microanalysis. *Microbeam Anal.*, **1985**: 104–106.
- Robert, J.-L., Bény, J.-M., Bény, C., Volfinger, M. (1989): Characterization of lepidolites by raman and infrared spectrometries. I. Relationships between OH-stretching wavenumbers and composition. *Can. Mineral.*, **27**, 225–235.
- Schreyer, W. & Seifert, F. (1969): High-pressure phases in the system $\text{MgO-Al}_2\text{O}_3\text{-SiO}_2\text{-H}_2\text{O}$. *Am. J. Sci.*, **267-A**, 407–443.
- Stahl, K., Kvik, Å., Smith, J.V. (1988): A neutron diffraction study of hydrogen positions at 13 k, domain model and chemical composition of staurolites. *J. Solid. State Chem.*, **73**, 362–380.
- Strens, R.G. (1974): The common chain, ribbon and ring silicates. In Farmer, V.C. (ed.): The infrared spectra of minerals. Min. Soc. London, 305–330.
- Turek, A., Riddle, C., Cozens, B.J., Tetley, N.W. (1976): Determination of chemical water in rock analysis by Karl-Fischer titration. *Chemical Geol.*, **17**, 261–267.
- Westrich, H.R. (1987): Determination of water in volcanic glasses by Karl-Fischer titration. *Chemical Geol.*, **63**, 335–340.

Received 5 May 1995

Modified version received 15 January 1996

Accepted 21 October 1996